Chemical Science

ROYAL SOCIETY OF CHEMISTRY

EDGE ARTICLE

View Article Online
View Journal | View Issue

Cite this: *Chem. Sci.*, 2025, **16**, 15004

All publication charges for this article have been paid for by the Royal Society of Chemistry

Molecular engineering of porphyrin dyes and copper complexes for enhanced dye regeneration toward high-performance dye-sensitized solar cells using copper(I/II) redox shuttles†

Yuzhe Zhang,[a] Tomohiro Higashino, *[a] Keigo Namikawa,[a] W. Ryan Osterloh[a] and Hiroshi Imahori *[abc]

Porphyrin dyes have garnered significant attention as promising photosensitizers for dye-sensitized solar cells (DSSCs) due to their exceptional light-harvesting capabilities and remarkable power conversion efficiencies (PCEs) when paired with cobalt(II/III) complex-based redox shuttles. Meanwhile, copper(I/II) complexes have emerged as new generation redox shuttles, achieving impressive open-circuit voltages (V_{OC}) exceeding 1.0 V. However, porphyrin-based DSSCs using copper(I/II) redox shuttles have struggled with low-to-moderate PCEs, primarily due to insufficient driving forces for the dye regeneration process. In this study, we introduce **FL1**, a novel porphyrin dye featuring a fluorene moiety with reduced electron-donating properties, designed to ensure a sufficient driving force for dye regeneration using copper(I/II) complexes. Under optimized conditions, DSSC incorporating **FL1** with a copper(I/II) complex utilizing 4,4′-dimethoxy-6,6′-dimethyl-2,2′-bipyridine **[Cu(2MeOby)$_2$][TFSI]/[Cu(2MeOby)$_2$][TFSI]$_2$** achieved a notable PCE of 8.30% with a V_{OC} of 0.890 V. Furthermore, our investigation into counterion effects revealed that DSSCs employing **[Cu(2MeOby)$_2$][PF$_6$]/[Cu(2MeOby)$_2$][PF$_6$]$_2$** as a redox shuttle delivered the highest PCE of 9.06% with a V_{OC} of 0.900 V, attributed to its superior diffusion coefficient. Finally, co-sensitized DSSCs featuring **FL1** and **XY1B** achieved an outstanding PCE of 10.9%, while retaining a high V_{OC} of 0.945 V, setting a new benchmark efficiency for porphyrin-based DSSCs utilizing copper(I/II) redox shuttles. This breakthrough highlights the immense potential of further refining porphyrin dyes and copper(I/II) redox shuttles through energy-level engineering to optimize the driving force for dye regeneration and propel advancements in DSSC technology.

Received 16th May 2025
Accepted 8th July 2025

DOI: 10.1039/d5sc03537f

rsc.li/chemical-science

Introduction

A substantial portion of global energy consumption still relies on fossil fuels, leading to substantial CO_2 emissions and pressing environmental concerns. This growing challenge has heightened the urgency for sustainable energy solutions, with solar energy emerging as a particularly compelling alternative, an abundant and virtually limitless resource derived from the sun. Among various solar technologies, organic solar cells present a promising avenue due to their cost-effective production, design flexibility, and lightweight properties.[1,2] Notably, dye-sensitized solar cells (DSSCs) have captured considerable attention due to their impressive high power conversion efficiencies (PCEs), vibrant multicolor fabrication possibilities, and outstanding performance under low-light conditions.[3–8]

Given the fundamental working principle of DSSCs, the sensitizer is a key player in facilitating light-harvesting and electron transfer (ET) processes at the dye/TiO_2/electrolyte interface. To push the boundaries of DSSC efficiency, the development of sensitizers with strong light-harvesting capabilities across the visible and near-infrared spectrum is highly desirable.[9–13] Moreover, the strategic incorporation of bulky substituents is crucial for suppressing charge recombination (CR) processes, thereby optimizing device performance. Porphyrin dyes have emerged as highly promising photosensitizers for DSSCs, thanks to their exceptional light-harvesting properties, adaptable electronic structures achieved through molecular engineering, and outstanding stability compared to conventional dyes.[14–32] Notably, single push-pull-type porphyrin

[a]*Department of Molecular Engineering, Graduate School of Engineering, Kyoto University, Kyoto, 615-8510, Japan. E-mail: t-higa@scl.kyoto-u.ac.jp; imahori@scl.kyoto-u.ac.jp*

[b]*Institute for Integrated Cell-Material Sciences (WPI-iCeMS), Kyoto University, Kyoto, 606-8501, Japan*

[c]*Institute for Liberal Arts and Sciences (ILAS), Kyoto University, Kyoto, 606-8316, Japan*

† Electronic supplementary information (ESI) available: Experimental section, synthetic details, optical and electrochemical properties of porphyrin dyes and copper complexes, photovoltaic properties, HR-MS spectra, and NMR spectra. CCDC 2451025–2451027. For ESI and crystallographic data in CIF or other electronic format see DOI: **https://doi.org/10.1039/d5sc03537f**

dyes designed with effective steric hindrance from bulky substituents have demonstrated impressive PCEs, reaching up to 13% when paired with tris(bipyridyl)$Co^{II/III}$ ($[Co(bpy)_3]^{2+/3+}$) as a redox shuttle. This progress underscores the immense potential of porphyrin-based sensitizers in advancing high-performance DSSCs.

Meanwhile, the redox shuttle serves as a crucial component in DSSCs, as the open-circuit voltage (V_{OC}) is primarily determined by the potential difference between the quasi-Fermi level of TiO_2 and the redox potential (E_{redox}) of the redox shuttle.[33–35] Over the past few decades, iodide/triiodide (I^-/I_3^-) and $[Co(bpy)_3]^{2+/3+}$ have been the most widely utilized redox shuttles. However, DSSCs incorporating these traditional shuttles have faced a V_{OC} limitation, with values restricted to below 1.0 V. To address this constraint, copper(I/II) complexes have emerged as new-generation redox shuttles, offering a more positive E_{redox} and significantly enhancing performance. DSSCs employing suitable complementary dyes and $\mathbf{[Cu(tmby)_2]^{+/2+}}$ (tmby = 4,4′-6,6′-dimethyl-2,2′-bipyridine) have achieved PCEs of up to 15%, coupled with a higher V_{OC} exceeding 1.0 V.[8,36–44] This progress emphasizes the transformative potential of copper-based redox shuttles in propelling DSSC efficiency to new heights.

In this context, DSSCs incorporating highly efficient porphyrin dyes alongside copper redox shuttles present a promising pathway for further enhancing PCE. However, despite their potential, the PCEs of porphyrin-based DSSCs using copper(I/II) complex-based redox shuttles remain below 7%, even in the case of **LG4** (Fig. 1),[45–47] falling significantly behind other organic dye-based DSSCs in performance. These low-to-moderate PCEs are primarily attributed to the challenge of achieving a sufficient driving force for effective dye regeneration ($-\Delta G_{reg} \geq 0.2$ eV). Conventional push–pull-type porphyrin dyes typically exhibit relatively low oxidation potentials (E_{ox}) of 0.7–0.8 V *vs.* NHE, limiting their compatibility with copper(I/II) complexes. In our previous studies, we demonstrated that increasing the $-\Delta G_{reg}$ value through energy-level engineering is an effective strategy for boosting PCEs in porphyrin-based DSSCs.[46] Thus, porphyrin dyes with elevated E_{ox} values (≥0.9 V *vs.* NHE) would be well-suited for DSSCs utilizing copper(I/II) complexes. Additionally, ligand modification of copper(I/II) complexes emerges as another promising approach for optimizing $-\Delta G_{reg}$ values (Fig. 2).[47,48] Incorporating electron-donating substituents into the bipyridine framework shifts the E_{redox} value negatively, a favorable adjustment for improving porphyrin-based DSSC performance. These advancements collectively pave the way for further refining porphyrin-copper systems, driving DSSCs toward higher efficiencies.

Herein, we present **FL1**, a novel porphyrin dye incorporating a 9,9-dioctylfluorene moiety, along with its photovoltaic

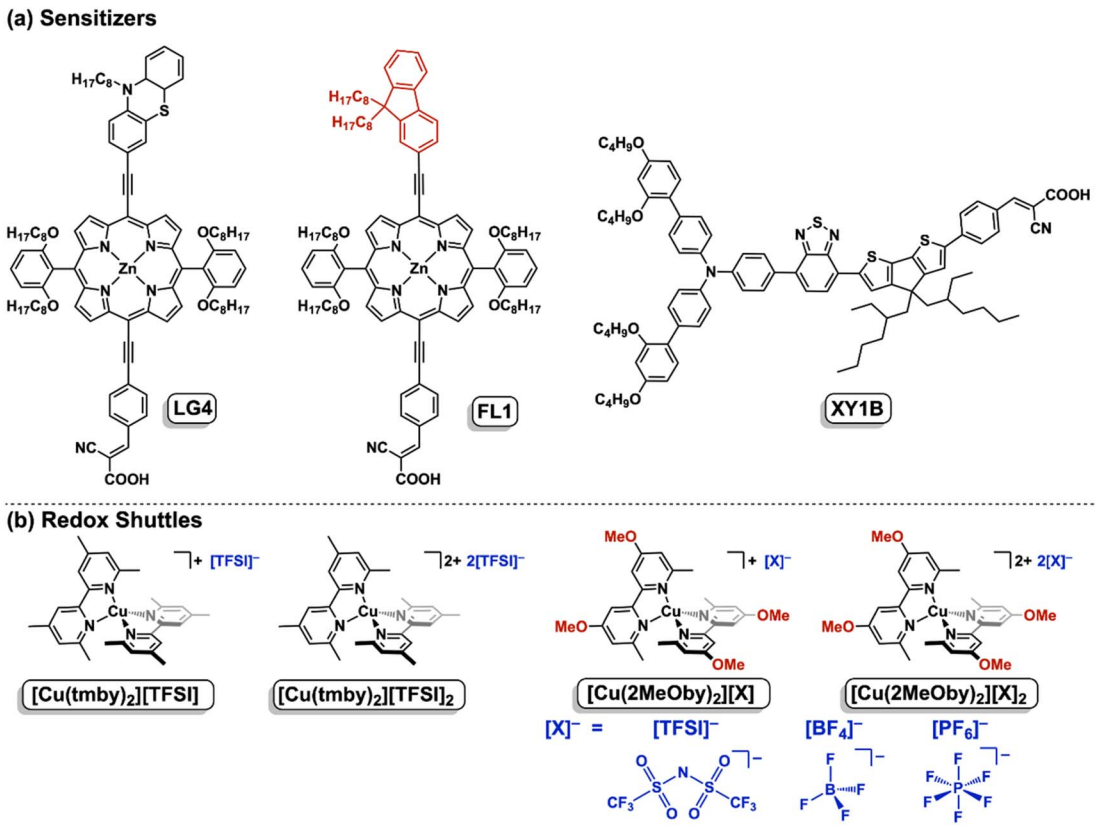

Fig. 1 Molecular structures of (a) porphyrin dyes **LG4** and **FL1** and co-sensitizer **XY1B**, and (b) copper complexes **[Cu(tmby)$_2$][TFSI]**, **[Cu(tmby)$_2$][TFSI]$_2$**, **[Cu(2MeOby)$_2$][X]**, and **[Cu(2MeOby)$_2$][X]$_2$**. The counterions ($[X]^-$) are trifluoromethanesulfonimide ($[TFSI]^-$), hexafluorophosphate ($[PF_6]^-$), and tetrafluoroborate ($[BF_4]^-$).

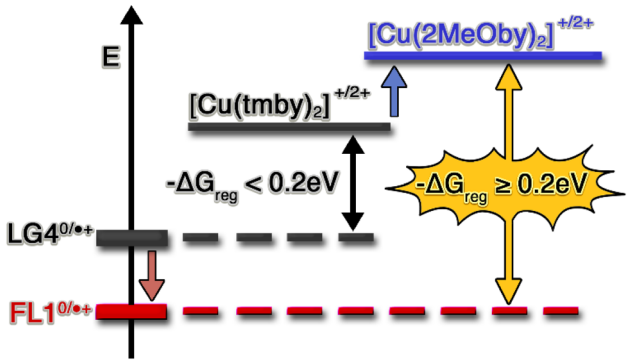

Fig. 2 Energy-level engineering of both dyes and redox shuttles for achieving an efficient driving force for dye regeneration ($-\Delta G_{reg}$) toward enhanced cell performance.

performance in DSSCs employing copper(I/II) complex-based redox shuttles (Fig. 1). The reduced electron-donating nature of the 9,9-dioctylfluorene moiety, compared to the phenothiazine moiety in previously reported **LG4**,[45] was expected to enhance the $-\Delta G_{reg}$ value (Fig. 2), while the two bulky octyl chains at the 9-position of the fluorene skeleton were anticipated to provide a strong blocking effect against the redox shuttle. Furthermore, we aimed to further increase the $-\Delta G_{reg}$ value by pairing **FL1** with a copper(I/II) complex incorporating 4,4′-dimethoxy-6,6′-dimethyl-2,2′-bipyridine (**2MeOby**), **[Cu(2MeOby)$_2$]$^{+/2+}$**, featuring electron-donating methoxy groups (Fig. 1). Additionally, we also investigated the effect of counterions because the counterion effect of the ruthenium dyes (*i.e.* **N719**) has been reported.[49] Actually, counterions play a critical role in the diffusion behavior of copper(I/II) complexes in organic solvents,[50] significantly influencing the PCE of DSSCs, as high diffusion coefficients are essential for efficient charge transport within the electrolyte.[50,51] To optimize charge transport, we examined three counterions, trifluoromethanesulfonimide ([TFSI]$^-$), tetrafluoroborate ([BF$_4$]$^-$), and hexafluorophosphate ([PF$_6$]$^-$). Through rational molecular engineering and a systematic exploration of the counterion effect, we successfully enhanced the PCE, with **FL1**-based DSSCs achieving an impressive PCE of 9.06%. Moreover, co-sensitization with **XY1B** further pushed the PCE beyond 10% while retaining a high V_{OC} of 0.945 V, marking the first instance of porphyrin-based DSSCs with copper(I/II) complex-based redox shuttles surpassing this milestone.

Results and discussion

Synthesis and characterization

The synthesis of the porphyrin dye **FL1** followed the procedure outlined in Scheme S1.† First, the Sonogashira coupling of 2-bromo-9,9′-dioctyl-9*H*-fluorene **1** (ref. 52) with triisopropylsilyl acetylene yielded ethynyl-substituted fluorene **2**. After deprotecting the silyl group with *n*-tetrabutylammonium fluoride (TBAF), subsequent Sonogashira coupling with *meso*-bromoporphyrin **3** (ref. 19) afforded bis-ethynyl substituted porphyrin **4**. Another round of triisopropylsilyl group deprotection enabled a final Sonogashira coupling with 4-iodobenzaldehyde to synthesize porphyrin **5**, which then underwent Knoevenagel condensation with cyanoacrylic acid to yield **FL1**.

Additionally, copper complexes incorporating [TFSI]$^-$ as a counterion were synthesized (Scheme S2†). The reaction of CuI with the ligand **2MeOby**,[53] followed by counterion exchange using LiTFSI, produced the copper(I) complex **[Cu(2MeOby)$_2$][TFSI]**. In contrast, the direct reaction of Cu(TFSI)$_2$ with **2MeOby** resulted in the copper(II) complex **[Cu(2MeOby)$_2$][TFSI]$_2$** without counterion exchange. Copper(I) complexes **[Cu(2MeOby)$_2$][X]** (X = BF$_4$ or PF$_6$) were obtained by reacting **[Cu(CH$_3$CN)$_4$][BF$_4$]** or **[Cu(CH$_3$CN)$_4$][PF$_6$]** with **2MeOby** (Scheme S3†). Meanwhile, the copper(II) complexes **[Cu(2MeOby)$_2$][X]$_2$** (X = BF$_4$ or PF$_6$) were prepared *via* a two-step process: first, $CuSO_4 \cdot 5H_2O$ was reacted with **2MeOby**, followed by counterion exchange with the respective ammonium salts (NH_4BF_4 or NH_4PF_6). Characterization of these compounds, including their copper complexes, was performed using ^{1}H and ^{13}C NMR, FT-IR spectroscopy, and high-resolution mass spectrometry (Fig. S1–S9†). Notably, the as-prepared copper(II) complexes contained varying proportions of their copper(I) counterparts due to unavoidable auto-reduction under ambient conditions, as Cl$^-$ ions were absent.[54,55] Since Kitagawa *et al.* reported that the auto-reduction of copper(II) complexes occurred in ethanol,[54] methanol in the reaction solvent may be a reductant for auto-reduction. On the other hand, we obtained pure copper(II) complexes by the bulk electrolysis of the corresponding copper(I) complexes, following established literature protocols.[56,57] The progress of electrochemical oxidation was monitored using the current, and the electrolysis was considered complete when the relative current approached zero, indicating that the copper(I) complexes had been entirely converted to their copper(II) counterparts (Fig. S16 and S17†). Since the as-prepared copper(II) complexes contain no other impurities except for the corresponding copper(I) complexes, the actual compositions of the as-prepared copper(II) complexes were determined as **[Cu(2MeOby)$_2$][X]$_n$** (n = 1.6–1.9; X = TFSI, BF$_4$, or PF$_6$) by absorbance at 748 nm in acetonitrile (Fig. S19†), using the absorption coefficient of pure copper(II) complexes (*vide infra*). It is noteworthy that the actual compositions of the as-prepared copper(II) complexes in our laboratory were also determined as **[Cu(tmby)$_2$][TFSI]$_{1.8}$** in a similar manner.

Single crystals suitable for X-ray diffraction analysis were successfully grown *via* vapor diffusion of Et$_2$O into acetonitrile solutions of **[Cu(2MeOby)$_2$][TFSI]** or **[Cu(2MeOby)$_2$][BF$_4$]** and by vapor diffusion of *n*-butanol into acetonitrile solutions of **[Cu(2MeOby)$_2$][PF$_6$]**. The resulting crystal structures (Fig. S10†) revealed Cu–N bond distances of 2.01–2.07 Å, confirming that the counterions had negligible influence on the geometry of the copper(I) complexes. The crystal data of the copper(I) complexes are also summarized in Table S1.†

Optical and electrochemical properties of porphyrin dyes

The UV/vis/NIR absorption spectra of the porphyrin dyes in tetrahydrofuran (THF) are presented in Fig. 3, with their optical properties summarized in Table 1. The absorption spectrum of

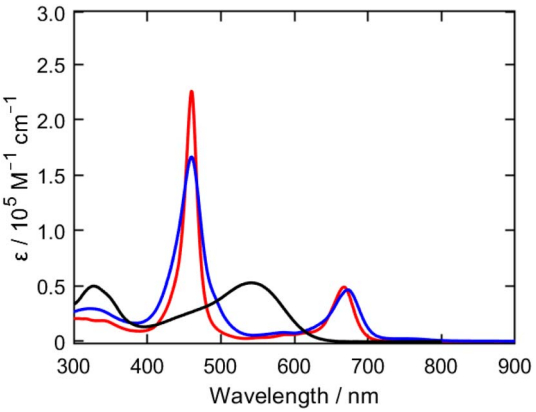

Fig. 3 UV/vis/NIR absorption spectra of **FL1** (red), **LG4** (blue), and **XY1B**[18] (black) in THF.

FL1 exhibits light-harvesting capabilities comparable to those of **LG4**, with a slight 5 nm blue-shift in its lowest-energy Q-band. This shift is attributed to the fluorene moiety's weaker electron-donating ability compared to the phenothiazine moiety in **LG4**. The steady-state fluorescence spectrum of **FL1** in THF also shows a 7 nm blue-shifted emission relative to **LG4**, aligning with the Q-band blue-shift observed in absorption spectra (Fig. S11†). The fluorescence lifetimes (τ), determined by time-correlated single-photon counting (TCSPC), are 1.3 ns for **FL1** and 1.2 ns for **LG4** (Fig. S12†). The almost identical lifetimes suggest that the replacement of the phenothiazine moiety with the fluorene moiety does not cause unfavorable aggregation tendency. The optical HOMO–LUMO gaps ($E_{0\text{–}0}$) of **FL1** and **LG4**, calculated from the intersection of their normalized absorption and emission spectra, are 1.90 eV and 1.87 eV, respectively (Table 1). Although the fluorene moiety is a weaker electron donor than the phenothiazine moiety, it has a minimal impact on **FL1**'s overall optical properties.

The electrochemical properties of the porphyrin dyes were evaluated using cyclic voltammetry (CV) and differential pulse voltammetry (DPV) in THF with 0.1 M tetrabutylammonium hexafluorophosphate (n-Bu_4NPF_6) as a supporting electrolyte. The first oxidation potential (E_{ox}) of **FL1** was measured at +0.93 V *vs.* NHE (Fig. S13†), which is more positive than that of **LG4** (+0.86 V *vs.* NHE), reinforcing the fluorene moiety's weaker electron-donating ability. To further assess the ET processes at the dye/TiO_2/electrolyte interface, CV measurements were performed for dye-adsorbed TiO_2 films (**FL1**/TiO_2 and **LG4**/TiO_2) as working electrodes. The E_{ox} values of **FL1**/TiO_2 and **LG4**/TiO_2 were determined to be +1.07 V and +0.98 V *vs.* NHE, respectively (Fig. S14† and Table 1). Considering the redox potential (E_{redox}) of the copper(I/II) complexes **[Cu(tmby)$_2$][TFSI]**/**[Cu(tmby)$_2$][TFSI]$_2$** (+0.88 V *vs.* NHE, Fig. S20a†), the driving forces for dye regeneration ($-\Delta G_{reg}$) of the porphyrin radical cation ($ZnP^{\bullet+}$) were calculated to be 0.19 eV for **FL1** and 0.10 eV for **LG4**. Since previous studies suggest that $-\Delta G_{reg}$ should be comparable to or larger than 0.20 eV for efficient dye regeneration *via* copper(I/II) redox shuttles,[36] the larger $-\Delta G_{reg}$ value for **FL1** than for **LG4** is expected to enhance dye regeneration efficiency, contributing to improved PCE. Additionally, the driving forces for electron injection ($-\Delta G_{inj}$) from the porphyrin excited singlet state (^{1}ZnP*) to the conduction band (CB) of TiO_2 (−0.5 V *vs.* NHE) were estimated using their excited-state oxidation potentials calculated using their oxidation potentials and optical HOMO–LUMO gaps. Both **FL1** and **LG4** possess sufficient $-\Delta G_{inj}$ values ($\geq$0.30 eV) to facilitate efficient electron injection into the CB of TiO_2.

To obtain insight into the ground state geometries and electronic structures of the porphyrin dyes, we performed density functional theory (DFT) calculations on model porphyrins at the B3LYP/6-31G(d) level (Fig. 4). Both **FL1** and **LG4** adopt a highly planar structure, facilitating an extended π-system for effective charge delocalization. The two alkyl chains at the 9-position of the fluorene moiety in **FL1** serve a dual purpose: providing a blocking effect and suppressing dye aggregation due to the enhanced steric hindrance (Fig. S15†). The highest occupied molecular orbitals (HOMOs) display significant orbital distribution on the porphyrin core and donor moieties, while the orbital distributions of the lowest unoccupied molecular orbitals (LUMOs) are mainly localized on the electron-withdrawing cyanoacrylic acid anchoring groups and porphyrin core. The HOMO level of **FL1** (−4.81 eV) is slightly more negative than that of **LG4** (−4.74 eV), agreeing with the weaker electron-donating ability of the fluorene moiety than the phenothiazine moiety. The calculated HOMO–LUMO energy gaps were determined to be 2.01 eV for **LG4** and 2.06 eV for **FL1**, aligning well with the optical HOMO–LUMO gaps and electrochemical properties of these porphyrin dyes.

Optical and electrochemical properties of copper complexes

The UV/vis/NIR absorption spectra of the copper complexes **[Cu(2MeOby)$_2$][X]** and **[Cu(2MeOby)$_2$][X]$_2$** (X = TFSI, BF_4, or PF_6) in acetonitrile are illustrated in Fig. S18,† with their optical

Table 1 Optical and electrochemical properties of porphyrin dyes

Dye	λ_{abs}[a]/nm (ε/10^3 M^{-1} cm^{-1})	λ_{em}[b]/nm	E_{ox}[c]/V	$E_{0\text{–}0}$/eV	E^*_{ox}[d]/V	$-\Delta G_{inj}$[e]/eV	$-\Delta G_{reg}$[f]/eV	$-\Delta G_{reg}$[g]/eV
FL1	460 (226), 668 (72)	681	1.07	1.90	−0.83	0.33	0.19	0.25
LG4	460 (206), 673 (69)	688	0.98	1.87	−0.89	0.39	0.10	0.16

[a] Wavelengths for Soret and Q-band maxima in THF. [b] Wavelengths for emission maxima in THF by excitation at Soret band maxima. [c] Determined by cyclic voltammetry (CV) measurements of the porphyrin-adsorbed TiO_2 films (*vs.* the normal hydrogen electrode (NHE)). [d] Determined by adding the $E_{0\text{–}0}$ value to the E_{ox} (*vs.* NHE). [e] Driving forces for electron injection from the porphyrin singlet excited state (^{1}ZnP*) to the conduction band (CB) of TiO_2 (−0.5 V *vs.* NHE). [f] Driving forces for the regeneration of oxidized porphyrin dyes ($ZnP^{\bullet+}$) by the **[Cu(tmby)$_2$]$^{+/2+}$** redox couple (+0.88 V *vs.* NHE). [g] Driving forces for the regeneration of oxidized porphyrin dyes ($ZnP^{\bullet+}$) by the **[Cu(2MeOby)$_2$]$^{+/2+}$** redox couple (+0.82 V *vs.* NHE).

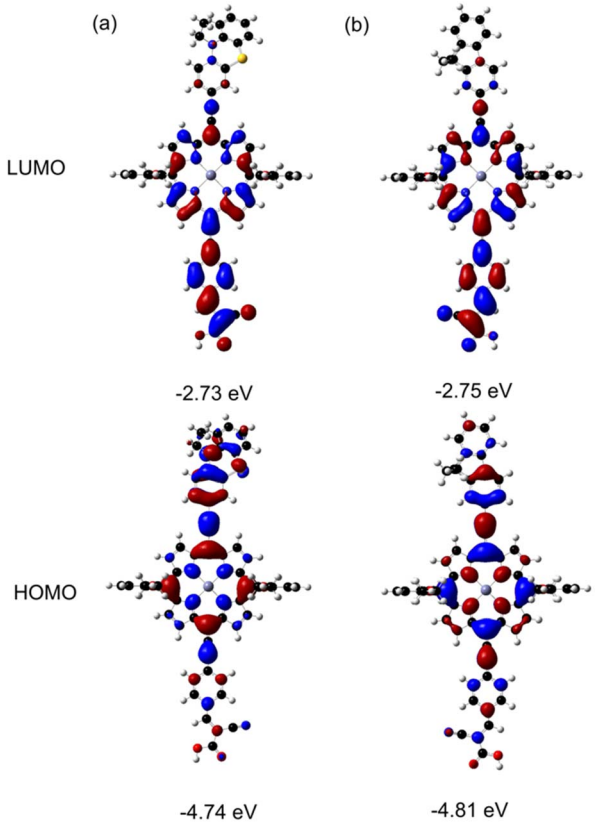

Fig. 4 Selected Kohn–Sham orbitals for (a) **LG4** and (b) **FL1** obtained using DFT calculations at the B3LYP/6-31G(d) level. To simplify the calculations, octyl groups on the donor side were replaced with ethyl groups and octyloxy groups on the *meso*-aryl groups were replaced with methoxy groups.

Table 2 Optical properties and diffusion coefficients of [Cu(2MeOby)$_2$][X] and [Cu(2MeOby)$_2$][X]$_2$ (X = TFSI, BF_4, or PF_6) in acetonitrile

	λ_{abs}[a]/nm (ε/M^{-1} cm^{-1})	D[b]/10^{-5} cm^2 s^{-1}
[Cu(2MeOby)$_2$][TFSI]	334 (4700), 445 (4500)	1.23
[Cu(2MeOby)$_2$][TFSI]$_2$	385 (1800), 748 (110)	—
[Cu(2MeOby)$_2$][BF$_4$]	334 (4500), 445 (4500)	1.30
[Cu(2MeOby)$_2$][BF$_4$]$_2$	385 (1700), 748 (130)	—
[Cu(2MeOby)$_2$][PF$_6$]	334 (4700), 445 (4600)	2.41
[Cu(2MeOby)$_2$][PF$_6$]$_2$	385 (1700), 748 (110)	—

[a] Wavelength of the absorption peaks in acetonitrile. [b] Diffusion coefficients determined *via* chronoamperometry.

properties detailed in Table 2. Although we obtained the pure copper(II) complexes *via* electrochemical oxidation of the corresponding copper(I) complexes (*vide supra*), we could not isolate the pure copper(II) complexes after electrolysis. Thus, we directly used the resulting solution for absorption and electrochemical measurements of the copper(II) complexes. The pronounced absorption bands spanning 300–500 nm are characteristic of metal-to-ligand charge transfer (MLCT) transitions, a defining feature of copper complexes. In contrast, the faint absorption observed at 748 nm arises from d–d transitions, a hallmark of copper(II) complexes.[54] Interestingly, **[Cu(2MeOby)$_2$][X]**/**[Cu(2MeOby)$_2$][X]$_2$** (X = TFSI, BF_4, or PF_6) exhibits identical absorption spectra, indicating that counter anions exert minimal influence on their optical properties.

To further explore the electrochemical behavior, we conducted CV measurements for both copper(I) and copper(II) complexes in acetonitrile (Fig. S20†). The copper(I) complex **[Cu(2MeOby)$_2$][TFSI]** displayed a reversible oxidation peak at +0.82 V *vs.* NHE. Notably, the copper(II) complex **[Cu(2MeOby)$_2$][TFSI]$_2$** exhibited a reversible reduction peak at precisely the same potential, +0.82 V, identical to the oxidation potential of its copper(I) counterpart. Consequently, the redox potential of **[Cu(2MeOby)$_2$][TFSI]**/**[Cu(2MeOby)$_2$][TFSI]$_2$** was determined to be +0.82 V *vs.* NHE, which is lower than that of **[Cu(tmby)$_2$][TFSI]**/**[Cu(tmby)$_2$][TFSI]$_2$** attributable to the electron-rich nature of the **2MeOby** ligand with methoxy substitutions. Furthermore, the redox potentials of **[Cu(2MeOby)$_2$][BF$_4$]**/**[Cu(2MeOby)$_2$][BF$_4$]$_2$** and **[Cu(2MeOby)$_2$][PF$_6$]**/**[Cu(2MeOby)$_2$][PF$_6$]$_2$** were similarly determined to be +0.82 V *vs.* NHE, reinforcing the notion that counterions have negligible impact on the redox behavior of the copper(I/II) complexes. Considering the E_{ox} values of **FL1**/TiO_2 (+1.07 V *vs.* NHE) and **LG4**/TiO_2 (+0.98 V *vs.* NHE), the $-\Delta G_{reg}$ values for **FL1** and **LG4** with **[Cu(2MeOby)$_2$]$^{+/2+}$** were estimated to be 0.25 and 0.16 eV, respectively. The increase in $-\Delta G_{reg}$ values is expected to accelerate the dye regeneration process, which, in turn, should enhance the PCE employing **[Cu(2MeOby)$_2$]$^{+/2+}$** as a redox shuttle.

Diffusion behavior of copper(I) complexes

The diffusion behavior of copper(I) complexes is closely linked to mass transport in DSSCs. Since charge transport in the electrolyte involves the movement of electroinactive counterions to maintain electroneutrality, the overall mass transport of copper(I/II) complexes is predominantly governed by their counterions.[51,58] The diffusion coefficients (D) of the copper(I) complexes were determined *via* chronoamperometry (Table 3 and Fig. S21†). For **[Cu(tmby)$_2$][TFSI]** and **[Cu(2MeOby)$_2$][TFSI]**, the measured diffusion coefficients were 1.28×10^{-5} and 1.23×10^{-5} cm^2 s^{-1}, respectively, aligning well with previous rotating disk electrode measurement for **[Cu(tmby)$_2$][TFSI]** (1.12×10^{-5} cm^2 s^{-1}).[39] This consistency suggests that the ligand structure has little influence on diffusion behavior. However, a notable deviation was observed for **[Cu(2MeOby)$_2$][PF$_6$]**, which exhibited a significantly higher diffusion coefficient of 2.41×10^{-5} cm^2 s^{-1}, compared to **[Cu(2MeOby)$_2$][TFSI]** and **[Cu(2MeOby)$_2$][BF$_4$]** (1.30×10^{-5} cm^2 s^{-1}). This enhanced diffusion is likely attributed to weak electrostatic interaction between the positively charged copper center and the negatively charged $[PF_6]^-$ counterion, facilitating superior mobility. Such favorable diffusion properties are essential for efficient charge transport within the electrolyte, even at low redox shuttle concentrations, ultimately supporting improved DSSC performance.

Table 3 Photovoltaic performances of the DSSCs using copper(I/II) complexes as redox shuttles under AM 1.5 illumination[a]

Dye	Electrolyte	J_{IPCE}[b]/mA cm^{-2}	J_{SC}/mA cm^{-2}	V_{OC}/V	ff	PCE/%
LG4	0.2 M **[Cu(tmby)$_2$][TFSI]** 0.05 M **[Cu(tmby)$_2$][TFSI]$_2$**	9.50 (0.7%)	9.57 (9.35 ± 0.4)	0.842 (0.844 ± 0.011)	0.716 (0.716 ± 0.003)	5.77 (5.65 ± 0.2)
LG4	0.2 M **[Cu(2MeOby)$_2$][TFSI]** 0.05 M **[Cu(2MeOby)$_2$][TFSI]$_2$**	10.0 (0.7%)	10.07 (9.96 ± 0.2)	0.821 (0.819 ± 0.002)	0.762 (0.763 ± 0.004)	6.30 (6.22 ± 0.1)
FL1	0.2 M **[Cu(tmby)$_2$][TFSI]** 0.05 M **[Cu(tmby)$_2$][TFSI]$_2$**	10.8 (3.5%)	11.2 (10.7 ± 0.6)	0.902 (0.895 ± 0.013)	0.767 (0.757 ± 0.019)	7.75 (7.28 ± 0.5)
FL1	0.2 M **[Cu(2MeOby)$_2$][TFSI]** 0.05 M **[Cu(2MeOby)$_2$][TFSI]$_2$**	12.3 (2.4%)	12.6 (12.1 ± 0.4)	0.887 (0.893 ± 0.01)	0.730 (0.719 ± 0.009)	8.15 (7.78 ± 0.3)
FL1	0.1 M **[Cu(tmby)$_2$][TFSI]** 0.025 M **[Cu(tmby)$_2$][TFSI]$_2$**	10.2 (1.9%)	10.4 (10.1 ± 0.4)	0.935 (0.919 ± 0.024)	0.720 (0.735 ± 0.03)	7.00 (6.84 ± 0.2)
FL1	0.1 M **[Cu(2MeOby)$_2$][TFSI]** 0.025 M **[Cu(2MeOby)$_2$][TFSI]$_2$**	11.6 (6.5%)	12.4 (12.3 ± 0.5)	0.890 (0.895 ± 0.006)	0.752 (0.748 ± 0.008)	8.30 (8.20 ± 0.2)
FL1	0.1 M **[Cu(2MeOby)$_2$][BF$_4$]** 0.025 M **[Cu(2MeOby)$_2$][BF$_4$]$_2$**	12.0 (4.7%)	12.6 (12.4 ± 0.6)	0.913 (0.916 ± 0.003)	0.777 (0.762 ± 0.02)	8.94 (8.63 ± 0.3)
FL1	0.1 M **[Cu(2MeOby)$_2$][PF$_6$]** 0.025 M **[Cu(2MeOby)$_2$][PF$_6$]$_2$**	13.0 (1.5%)	13.2 (12.7 ± 0.4)	0.900 (0.910 ± 0.01)	0.763 (0.762 ± 0.006)	9.06 (8.80 ± 0.2)
XY1B	0.1 M **[Cu(2MeOby)$_2$][PF$_6$]** 0.025 M **[Cu(2MeOby)$_2$][PF$_6$]$_2$**	14.1 (2.1%)	14.4 (14.6 ± 0.2)	0.961 (0.963 ± 0.002)	0.752 (0.73 ± 0.02)	10.4 (10.3 ± 0.1)
FL1 + **XY1B**	0.1 M **[Cu(2MeOby)$_2$][PF$_6$]** 0.025 M **[Cu(2MeOby)$_2$][PF$_6$]$_2$**	14.4 (5.3%)	15.2 (15.3 ± 0.1)	0.945 (0.940 ± 0.01)	0.756 (0.752 ± 0.005)	10.9 (10.8 ± 0.1)

[a] Photovoltaic parameters derived from the highest PCEs. The values in parentheses denote average values from three or four independent experiments. Error bars represent the standard error of the mean. [b] The J_{IPCE} values were obtained by integrating the IPCE plots, and the relative discrepancies from the corresponding J_{SC} values obtained from the *J–V* characteristics are provided in the parentheses.

Photovoltaic properties of DSSCs with FL1 and LG4 using [Cu(tmby)$_2$][TFSI]/[Cu(tmby)$_2$][TFSI]$_2$ and [Cu(2MeOby)$_2$][TFSI]/[Cu(2MeOby)$_2$][TFSI]$_2$ as redox shuttles

To optimize the fabrication conditions for DSSCs with **FL1** under standard AM 1.5 conditions, we first utilized **[Cu(tmby)$_2$][TFSI]/[Cu(tmby)$_2$][TFSI]$_2$** as a redox shuttle. Because the as-prepared copper(II) complex contains no other impurities except for the corresponding copper(I) species (*vide supra*), we can prepare the electrolyte solution with an accurate concentration by adjusting the amounts of copper(I/II) complexes based on the actual composition of the copper(II) complex **[Cu(tmby)$_2$][TFSI]$_{1.8}$**. The electrolyte solution consisted of 0.2 M **[Cu(tmby)$_2$][TFSI]**, 0.05 M **[Cu(tmby)$_2$][TFSI]$_2$**, 0.1 M LiTFSI, and 0.5 M 4-*tert*-butylpyridine (TBP) in acetonitrile. We screened immersion solvents while maintaining a fixed immersion time of 3 hours, ultimately selecting a mixture of toluene and ethanol (EtOH) in a 1 : 5 v/v ratio. We then evaluated the effect of immersion time, observing that PCEs increased with extended immersion periods, reaching a peak value of 6.94% for **FL1** at 3 hours (Fig. S22†). To further enhance performance, we investigated chenodeoxycholic acid (CDCA) as a co-adsorbent to suppress dye aggregation on TiO_2 (Fig. S23†). The DSSC employing **FL1** achieved a maximum PCE of 7.75% upon the addition of 1 equivalent of CDCA. For a comparative analysis, we fabricated DSSCs with **LG4**-sensitized TiO_2 films under previously optimized conditions.[46] The DSSC with **LG4** using **[Cu(tmby)$_2$][TFSI]/[Cu(tmby)$_2$][TFSI]$_2$** exhibited a lower PCE of 5.77%, significantly below that with **FL1**. Notably, the optimized CDCA concentration was 1 equivalent for **FL1** but 4 equivalents for **LG4**, likely due to **FL1**'s reduced aggregation tendency arising from steric hindrance by its two alkyl chains at the 9-position of the fluorene moiety. Additionally, we fabricated DSSCs utilizing **[Cu(2MeOby)$_2$][TFSI]/[Cu(2MeOby)$_2$][TFSI]$_2$** as a redox shuttle, benefiting from its larger $-\Delta G_{reg}$ values due to the less positive E_{redox} value (Table 1). The DSSCs employing **[Cu(2MeOby)$_2$][TFSI]/[Cu(2MeOby)$_2$][TFSI]$_2$** demonstrated superior PCEs (8.15% for **FL1** and 6.30% for **LG4**) compared to those using **[Cu(tmby)$_2$][TFSI]/[Cu(tmby)$_2$][TFSI]$_2$**. While DSSCs with **[Cu(2MeOby)$_2$][TFSI]/[Cu(2MeOby)$_2$][TFSI]$_2$** exhibited slightly lower V_{OC} values due to the less positive E_{redox} value, the enhanced J_{SC} values effectively compensated for this decrease, ultimately resulting in improved PCEs.

The photocurrent–voltage characteristics of DSSCs under optimized conditions are presented in Fig. 5, with the corresponding photovoltaic data listed in Table 3. The superior PCEs observed for **FL1** compared to **LG4** primarily stem from its higher J_{SC} and V_{OC} values. The enhanced J_{SC} values are attributed to improved incident photon-to-current efficiencies (IPCEs), as illustrated in Fig. 6b. The IPCE values follow the trend: **LG4** with **[Cu(tmby)$_2$][TFSI]/[Cu(tmby)$_2$][TFSI]$_2$** < **LG4** with **[Cu(2MeOby)$_2$][TFSI]/[Cu(2MeOby)$_2$][TFSI]$_2$** < **FL1** with **[Cu(tmby)$_2$][TFSI]$_2$/[Cu(tmby)$_2$][TFSI]$_2$** < **FL1** with **[Cu(2MeOby)$_2$][TFSI]/[Cu(2MeOby)$_2$][TFSI]$_2$**. Indeed, the J_{IPCE} values derived from photocurrent action spectra are compatible with the measured J_{SC} values. To further elucidate the differences in IPCE, we analyzed light-harvesting efficiency (LHE), electron injection efficiency (ϕ_{inj}), and charge collection efficiency (η_{col}), based on the equation: IPCE = LHE × ϕ_{inj} × η_{col}. The absorption spectra of dye-adsorbed TiO_2 films, recorded without a light-scattering layer, revealed nearly identical absorption profiles for **FL1** and **LG4** (Fig. 6a). Taking into account the excellent absorption coefficients of the porphyrin dyes and the presence of a light-scattering layer in the actual

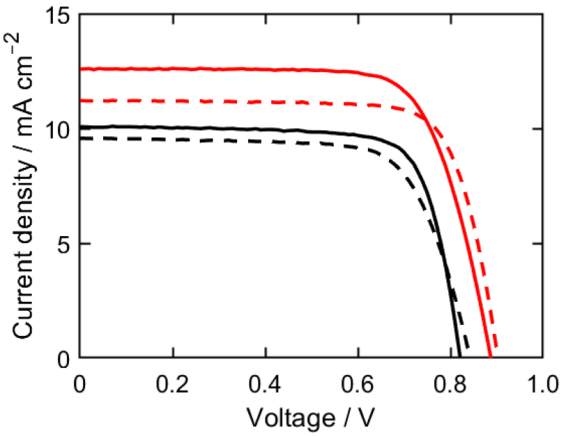

Fig. 5 Photocurrent–voltage characteristics of the DSSCs with **FL1** (red) and **LG4** (black) using **[Cu(tmby)$_2$][TFSI]/[Cu(tmby)$_2$][TFSI]$_2$** (dashed lines) and **[Cu(2MeOby)$_2$][TFSI]/[Cu(2MeOby)$_2$][TFSI]$_2$** (solid lines) redox shuttles for achieving the highest PCEs under the optimized conditions. The composition of the electrolyte solution: 0.2 M **[CuL$_2$][TFSI]**, 0.05 M **[CuL$_2$][TFSI]$_2$**, 0.1 M LiTFSI, and 0.5 M TBP in acetonitrile (**L** = **tmby** or **2MeOby**).

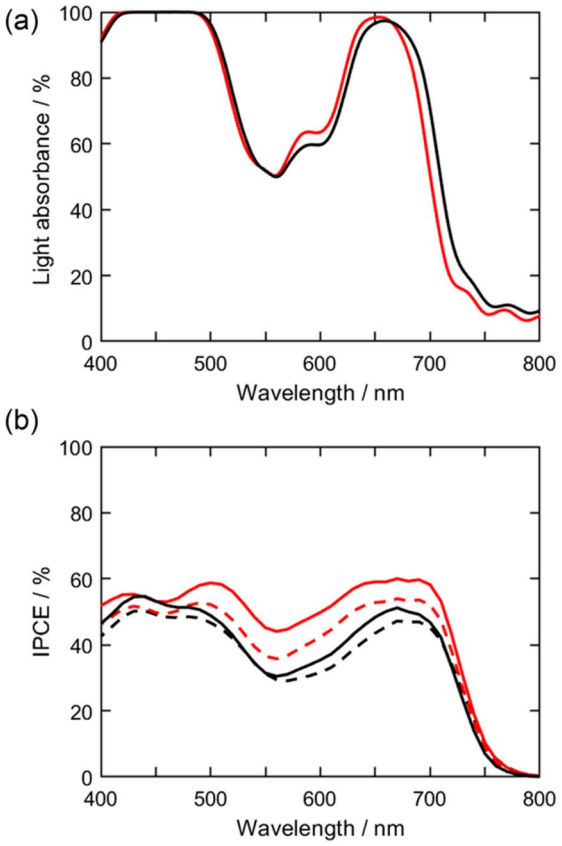

Fig. 6 (a) Absorption spectra of the porphyrin-adsorbed TiO_2 film (2 μm) of **FL1** (red) and **LG4** (black), and (b) photocurrent action spectra of the DSSCs with **FL1** (red) and **LG4** (black) using **[Cu(tmby)$_2$][TFSI]/[Cu(tmby)$_2$][TFSI]$_2$** (dashed lines) and **[Cu(2MeOby)$_2$][TFSI]/[Cu(2MeOby)$_2$][TFSI]$_2$** (solid lines) redox shuttles. The light-scattering TiO_2 layers were not used to obtain an accurate absorption profile for the light-harvesting efficiency.

device, the LHE values approach 100% for both dyes. Although self-quenching of the excited state due to dye aggregation on TiO_2 could potentially reduce ϕ_{inj}, co-adsorption of CDCA effectively mitigates dye aggregation effects. Consequently, the higher IPCE values observed for **FL1** compared to **LG4** are primarily attributed to its superior η_{col} values.

Given that the η_{col} value correlates with the dye regeneration efficiency (φ_{reg}), we conducted microsecond time-resolved transient absorption (TA) measurements on the porphyrin-sensitized TiO_2 films. The decay profiles of the porphyrin radical cation ($ZnP^{\bullet+}$) at 800 nm were analyzed, as the electrochemical oxidation of the porphyrin dyes distinctly revealed the characteristic absorption at 700–850 nm (Fig. S24†). The φ_{reg} values were derived from the lifetimes of $ZnP^{\bullet+}$ in the absence and presence of copper(I/II) redox shuttles (Fig. S25 and Table S2†). The estimated φ_{reg} values follow the trend: **LG4** with **[Cu(tmby)$_2$][TFSI]/[Cu(tmby)$_2$][TFSI]$_2$** (58%) < **LG4** with **[Cu(2-MeOby)$_2$][TFSI]/[Cu(2MeOby)$_2$][TFSI]$_2$** (66%) < **FL1** with **[Cu(tmby)$_2$][TFSI]/[Cu(tmby)$_2$][TFSI]$_2$** (71%) < **FL1** with **[Cu(2MeOby)$_2$][TFSI]/[Cu(2MeOby)$_2$][TFSI]$_2$** (84%). This order aligns well with the trend observed for the $-\Delta G_{reg}$ values. The highest φ_{reg} value of 84% for **FL1** with **[Cu(2MeOby)$_2$][TFSI]/[Cu(2MeOby)$_2$][TFSI]$_2$** underscores the critical role of achieving a $-\Delta G_{reg}$ value of 0.2 eV for an efficient dye regeneration process, even in DSSCs employing copper(I/II) redox shuttles.

To further assess CR between electrons in the CB of TiO_2 and the redox shuttle, we examined current–voltage characteristics under dark conditions (Fig. S26†). The more positive voltage onsets observed for **FL1** compared to **LG4** indicate an effective suppression of the CR process, likely due to an enhanced blocking effect. Dye loading amounts (Γ) for **FL1** and **LG4**, under the optimized sensitization conditions, were determined to be 9.5×10^{-11} and 1.1×10^{-10} mol cm^{-2}, respectively. These values were obtained by measuring the absorbance of porphyrin dyes dissolved from the dye-sensitized TiO_2 films into a THF/H_2O (v/v = 1/1) solution with 0.1 M NaOH. The smaller Γ value for **FL1** compared to **LG4** suggests that the increased steric hindrance of **FL1** plays a critical role in enhancing the blocking effect and suppressing dye aggregation on TiO_2, primarily due to the presence of alkyl chains on the fluorene moiety. Additionally, the ET process at the dye/TiO_2/electrolyte interface was investigated using electrical impedance spectroscopy (EIS) under AM 1.5 illumination under open-circuit conditions (Fig. S27†). The charge transfer resistance (R_p) at the TiO_2/dye/electrolyte interface followed this trend: (32.2 Ω for **LG4** with **[Cu(2MeOby)$_2$][TFSI]/[Cu(2MeOby)$_2$][TFSI]$_2$** < 36.8 Ω for **LG4** with **[Cu(tmby)$_2$][TFSI]/[Cu(tmby)$_2$][TFSI]$_2$** < 42.5 Ω for **FL1** with **[Cu(2MeOby)$_2$][TFSI]/[Cu(2MeOby)$_2$][TFSI]$_2$** < 45.0 Ω for **FL1** with **[Cu(tmby)$_2$][TFSI]/[Cu(tmby)$_2$][TFSI]$_2$**). This order is consistent with that of the observed V_{OC} values, reinforcing the correlation between increased R_p values for **FL1** and higher V_{OC} values in the DSSC utilizing **FL1** compared to **LG4**.

To demonstrate the potential of our new porphyrin dye **FL1** for DSSCs using copper(I/II) complex-based redox shuttles, we also measured photovoltaic performances of the DSSCs with **FL1** and **LG4** using the standard I^-/I_3^- redox shuttle (Fig. S28, S29 and Table S3†). Although the DSSCs using the I^-/I_3^- redox

shuttle exhibited higher J_{SC} values than those using **[Cu(L)$_2$][TFSI]/[Cu(L)$_2$][TFSI]$_2$** (**L** = **tmby** or **2MeOby**) due to their larger driving forces for dye regeneration, the less positive redox potential of I^-/I_3^- (+0.40 V *vs.* NHE) resulted in significantly lower V_{OC} values. Overall, the PCEs of the DSSCs using the I^-/I_3^- redox shuttle (5.84% for **LG4** and 6.74% for **FL1**) are lower than those using the **[Cu(2MeOby)$_2$][TFSI]/[Cu(2MeOby)$_2$][TFSI]$_2$** redox shuttle. These results clearly corroborate that the combination of the porphyrin dye and the copper(I/II) complex-based redox shuttle with a sufficient $-\Delta G_{reg}$ value is an effective means to achieve further enhancement in PCE.

Effect of electrolyte composition on photovoltaic performances

The electrolyte solution plays a crucial role in DSSCs, prompting an investigation into the effect of its composition, specifically the concentration and counterions, on the photovoltaic properties of DSSCs with **FL1**. We first examined the performance using a low-concentration electrolyte containing 0.1 M **[CuL$_2$][TFSI]** and 0.025 M **[CuL$_2$][TFSI]$_2$** (**L** = **tmby** or **2MeOby**) for **[Cu(tmby)$_2$][TFSI]/[Cu(tmby)$_2$][TFSI]$_2$** and **[Cu(2MeOby)$_2$][TFSI]/[Cu(2MeOby)$_2$][TFSI]$_2$**. The DSSC employing **[Cu(2MeOby)$_2$][TFSI]/[Cu(2MeOby)$_2$][TFSI]$_2$** exhibited a slight improvement in PCE (8.30%), whereas the DSSC with **[Cu(tmby)$_2$][TFSI]/[Cu(tmby)$_2$][TFSI]$_2$** showed a significant decrease in PCE (7.00%) (Fig. S30† and Table 3). Reducing the concentration of copper(I/II) complexes led to a slight increase in the V_{OC} values likely due to suppressed CR between electrons in TiO_2 and the redox shuttle. Interestingly, the J_{SC} value of the DSSC using **[Cu(2MeOby)$_2$][TFSI]/[Cu(2MeOby)$_2$][TFSI]$_2$** remained comparable across both low and high concentrations, suggesting its robustness. In contrast, the J_{SC} value for **[Cu(tmby)$_2$][TFSI]/[Cu(tmby)$_2$][TFSI]$_2$** decreased substantially, directly contributing to its lower PCE. Considering the similar diffusion coefficients of **[Cu(tmby)$_2$][TFSI]** and **[Cu(2MeOby)$_2$][TFSI]**, the diminished J_{SC} value for **[Cu(tmby)$_2$][TFSI]/[Cu(tmby)$_2$][TFSI]$_2$** at low concentrations can likely be ascribed to an inefficient dye regeneration process. Therefore, achieving higher $-\Delta G_{reg}$ values proves advantageous for DSSCs operating with low-concentration electrolytes.

Since counterions significantly affect diffusion properties (*vide supra*), they are also expected to impact the photovoltaic performance of DSSCs utilizing copper(I/II) complexes. To investigate this effect, we examined different counterions at optimal concentrations of 0.1 M **[Cu(2MeOby)$_2$][X]** and 0.025 M **[Cu(2MeOby)$_2$][X]$_2$** (X = TFSI, BF_4, or PF_6) (Fig. 7a and Table 3). DSSCs incorporating **[Cu(2MeOby)$_2$][X]/[Cu(2MeOby)$_2$][X]$_2$** (X = BF_4 or PF_6) attained higher PCEs (8.94% for **[Cu(2MeOby)$_2$][BF$_4$]/[Cu(2MeOby)$_2$][BF$_4$]$_2$** and 9.06% for **[Cu(2MeOby)$_2$][PF$_6$]/[Cu(2MeOby)$_2$][PF$_6$]$_2$**) compared to **[Cu(2MeOby)$_2$][TFSI]/[Cu(2MeOby)$_2$][TFSI]$_2$**. Remarkably, the PCE of the DSSC employing **FL1** with **[Cu(2MeOby)$_2$][PF$_6$]/[Cu(2MeOby)$_2$][PF$_6$]$_2$** is the highest reported among porphyrin-based DSSCs with copper(I/II) redox shuttles. The superior PCE observed for **[Cu(2MeOby)$_2$][PF$_6$]/[Cu(2MeOby)$_2$][PF$_6$]$_2$** can be attributed to its significantly improved J_{SC} value, in line with its higher IPCE values relative to those of **[Cu(2MeOby)$_2$][BF$_4$]/[Cu(2MeOby)$_2$][BF$_4$]$_2$** and **[Cu(2MeOby)$_2$][TFSI]/[Cu(2MeOby)$_2$][TFSI]$_2$** (Fig. 7b). To further elucidate this enhancement, we estimated φ_{reg} values through time-resolved TA measurements conducted in the presence of copper(I/II) complexes at low concentrations (0.1 M Cu^I and 0.025 M Cu^{II}) (Fig. S31 and Table S4†). The φ_{reg} values followed the trend: **[Cu(2MeOby)$_2$][TFSI]/[Cu(2MeOby)$_2$][TFSI]$_2$** (83%) < **[Cu(2MeOby)$_2$][BF$_4$]/[Cu(2MeOby)$_2$][BF$_4$]$_2$** (84%) < **[Cu(2MeOby)$_2$][PF$_6$]/[Cu(2MeOby)$_2$][PF$_6$]$_2$** (87%). Since counterions do not directly impact the E_{redox} value, the highest diffusion coefficient of **[Cu(2MeOby)$_2$][PF$_6$]** is likely responsible for the superior φ_{reg}, IPCE, and J_{SC} values, ultimately leading to the highest PCE. Even though the maximum IPCE value of the DSSC using **[Cu(2MeOby)$_2$][PF$_6$]/[Cu(2MeOby)$_2$][PF$_6$]$_2$** exceeded 60% due to the highest φ_{reg} value, there remains room for further improvement in the J_{SC} value. Considering that the enhanced blocking effect can suppress the unfavorable CR process,[17,18] the introduction of bulky substituents is expected to increase the η_{col} value, leading to a higher J_{SC} value.

We also measured current–voltage characteristics under dark conditions (Fig. S32†) to evaluate the impact of counterions on V_{OC} values. The onsets of dark current for **[Cu(2MeOby)$_2$][BF$_4$]/[Cu(2MeOby)$_2$][BF$_4$]$_2$** and **[Cu(2MeOby)$_2$][PF$_6$]/[Cu(2MeOby)$_2$][PF$_6$]$_2$** were more positive than those for **[Cu(2MeOby)$_2$][TFSI]/[Cu(2MeOby)$_2$][TFSI]$_2$**. Thus, the slightly improved V_{OC} values observed for **[Cu(2MeOby)$_2$][BF$_4$]/[Cu(2MeOby)$_2$][BF$_4$]$_2$** and **[Cu(2MeOby)$_2$][PF$_6$]/[Cu(2MeOby)$_2$][PF$_6$]$_2$** can be ascribed to more effective suppression of CR between electrons in the CB of TiO_2 and the redox shuttle. Although the precise mechanism remains unclear at this stage, these findings suggest that counterions significantly influence interfacial behavior at the TiO_2/dye/electrolyte interfaces, with the $[TFSI]^-$ anion potentially accelerating undesirable CR processes.

Photovoltaic properties of co-sensitized DSSCs with XY1B

The DSSC with **FL1** using **[Cu(2MeOby)$_2$][PF$_6$]/[Cu(2MeOby)$_2$][PF$_6$]$_2$** achieved the highest PCE among porphyrin-based DSSCs with copper(I/II) redox shuttles. However, further improvement in J_{SC} values and overall PCEs remains possible due to relatively low IPCE values at around 550 nm. Co-sensitization with additional dyes exhibiting complementary absorption properties presents an effective strategy for achieving panchromatic absorption by addressing absorption deficits.[59–61] To this end, we selected **XY1B** as a co-sensitizer, considering its excellent absorption profile (ε = 53 000 M^{-1} cm^{-1} at 541 nm)[18] and high PCE (10.4%) in DSSCs under our optimized conditions (Fig. 2, S33† and Table 3). The co-sensitized TiO_2 films were prepared *via* a second immersion step, wherein **FL1**-sensitized TiO_2 films were immersed in an **XY1B** solution (0.1 M, 50 equiv. CDCA) in THF and ethanol solution (v/v = 1/4). Following optimization of the second immersion conditions, the co-sensitized DSSC with **FL1** + **XY1B** exhibited an enhanced PCE, driven by improved J_{SC} and V_{OC} values (Fig. 7a and Table 3). The photocurrent action spectra clearly demonstrate a substantial increase in IPCE values within the 500–600 nm range, reaching 69% after co-sensitization with **XY1B** (Fig. 7b).

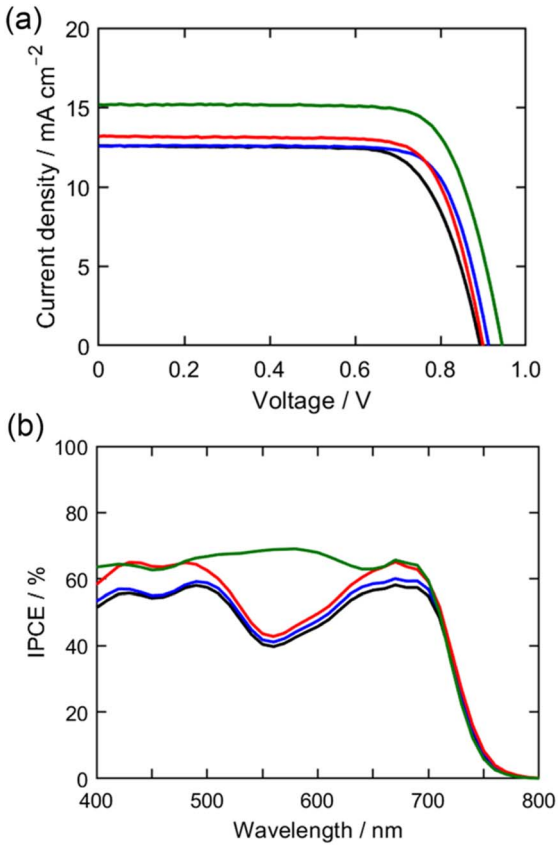

Fig. 7 (a) Photocurrent–voltage characteristics and (b) photocurrent action spectra of the DSSCs with **FL1** using [Cu(2MeOby$_2$][TFSI]/[Cu(2MeOby$_2$][TFSI]$_2$ (black), [Cu(2MeOby$_2$][BF$_4$]/[Cu(2MeOby$_2$][BF$_4$]$_2$ (blue), and [Cu(2MeOby$_2$][PF$_6$]/[Cu(2MeOby$_2$][PF$_6$]$_2$ (red) and the DSSC with **FL1** + **XY1B** using [Cu(2MeOby$_2$][PF$_6$]/[Cu(2MeOby$_2$][PF$_6$]$_2$ (green) under the optimized conditions for achieving the highest PCEs. The composition of the electrolyte solution: 0.1 M [Cu(2MeOby$_2$][X], 0.025 M [Cu(2MeOby$_2$][X]$_2$, 0.1 M LiX, and 0.5 M TBP in acetonitrile (X = TFSI, BF$_4$, or PF$_6$).

This enhancement is corroborated by increased absorption observed in co-sensitized TiO_2 films at approximately 550 nm (Fig. S34†). Dye loading amounts of **FL1** and **XY1B** on the co-sensitized TiO_2 were determined to be 4.7×10^{-11} and 6.2×10^{-11} mol cm^{-2}, respectively, confirming that the J_{SC} enhancement stems from the complementary absorption of **XY1B**. Furthermore, current–voltage characteristics of the co-sensitized DSSC under dark conditions displayed a positive shift in the onset voltage, agreeing with the observed increase in V_{OC} (Fig. S32†). Ultimately, the co-sensitized DSSC with **FL1** + **XY1B** attained an outstanding PCE of 10.9%, surpassing the highest PCE recorded for porphyrin-based DSSCs employing copper(I/II) redox shuttles, marking the first instance of exceeding 10% PCE. Since the V_{OC} value (0.945 V) is slightly higher than the highest V_{OC} value in the co-sensitized porphyrin-based DSSCs with $[Co(bpy)_3]^{2+/3+}$ (0.935 V),[19] further optimization of device fabrication conditions will achieve a V_{OC} value higher than 1.0 V. In contrast, the co-sensitized DSSC with **LG4** + **XY1B** delivered a PCE of 8.40%, which fell below that with **XY1B** as a single dye (Fig. S35 and Table S5†). This reduction may be attributed to **LG4**'s aggregation tendency, which likely quenches **XY1B**'s excited state, thereby impairing performance. Notably, the two alkyl chains on the fluorene moiety of **FL1** play a crucial role in suppressing dye aggregation, proving advantageous not only for aggregation control but also for co-sensitization.

Stability of the DSSCs

The long-term stability of the DSSCs was assessed under white-light illumination (100 mW cm^{-2}) at 25 °C over a 500-hour period. The DSSC with **FL1** + **XY1B** retained 84% of its initial efficiency, outperforming the DSSC with **LG4** + **XY1B**, which maintained 73% (Fig. S36†). The superior stability of **FL1** + **XY1B** may have resulted from the weaker electron-donating ability of the fluorene moiety in **FL1** relative to the phenothiazine moiety in **LG4**, a characteristic beneficial for practical use.

Conclusions

We designed and synthesized a novel porphyrin dye, **FL1**, incorporating a fluorene skeleton with a weaker electron-donating nature relative to the phenothiazine skeleton. The E_{ox} value of **FL1**/TiO_2 was determined to be +1.07 V *vs.* NHE, ensuring a $-\Delta G_{reg}$ value comparable to or larger than 0.2 eV. Thanks to this increased $-\Delta G_{reg}$ value, the DSSC with **FL1** achieved a higher PCE of 7.75% than that with **LG4** (5.77%) when using **[Cu(tmby)$_2$][TFSI]/[Cu(tmby)$_2$][TFSI]$_2$** as the redox shuttle. Furthermore, the DSSC with **FL1** employing **[Cu(2MeOby)$_2$][TFSI]/[Cu(2MeOby)$_2$][TFSI]$_2$** exhibited an even higher PCE of 8.15%, attributed to an increased $-\Delta G_{reg}$ value (0.25 eV). This finding underscores the importance of maintaining sufficient $-\Delta G_{reg}$ values for achieving high-performance porphyrin-based DSSCs using copper(I/II) redox shuttles. To further explore performance optimization, we investigated the influence of counterions in **[Cu(2MeOby)$_2$][X]/[Cu(2MeOby)$_2$][X]$_2$** (X = TFSI, BF_4, or PF_6) on diffusion behavior and identified **[Cu(2MeOby)$_2$][PF$_6$]** as having the highest diffusion coefficient. Consequently, the DSSC with **FL1** using **[Cu(2MeOby)$_2$][PF$_6$]/[Cu(2MeOby)$_2$][PF$_6$]$_2$** attained the highest PCE of 9.06%, creating a new benchmark for porphyrin-based DSSCs employing copper(I/II) complex-based redox shuttles. Notably, co-sensitized DSSC with **FL1** and the complementary dye **XY1B** led to an impressive PCE of 10.9%, while maintaining a high V_{OC} of 0.945 V, setting a groundbreaking record as the first porphyrin-based DSSC employing copper(I/II) complex-based redox shuttles to exceed 10% PCE. Overall, our findings confirm that rational molecular engineering of porphyrin dyes and copper(I/II) complex-based redox shuttles with sufficient $-\Delta G_{reg}$ values can significantly enhance photovoltaic performance. Additionally, selecting appropriate counterions with high diffusion coefficients is crucial for maximizing the charge transporting capabilities of copper(I/II) complexes. We anticipate that further refinement of porphyrin-based DSSCs, complementary dyes, and copper(I/II) redox shuttles through energy-level engineering will pave the way for next-generation solar cell technology, driving it toward top-tier performance.

Data availability

The data supporting this article have been included as part of the ESI.†

Author contributions

T. Higashino and H. Imahori conceived and designed this work. Y. Zhang and K. Namikawa conducted the synthesis and characterization of the products. Y. Zhang, K. Namikawa, and W. R. Osterloh performed spectroscopic and electrochemical measurements. Y. Zhang fabricated the DSSCs and evaluated their photovoltaic performances. Y. Zhang, T. Higashino, and H. Imahori co-wrote the manuscript.

Conflicts of interest

There are no conflicts to declare.

Acknowledgements

This work was supported by the JSPS (KAKENHI Grant Numbers JP20H05841 (T. H.), JP22K05066 (T. H.), JP25K01874 (T. H.), JP20H05832 (H. I.), and JP23H00309 (H. I.)). Y. Z. thanks the China Scholarship Council (CSC) (Chinese Government Scholarship 202006250042) for funding. In this work, DFT calculations were performed using the supercomputer of ACCMS under the collaborative research program for young/women scientists, Kyoto University.

Notes and references

1 E. K. Solak and E. Irmak, *RSC Adv.*, 2023, **13**, 12244–12269.
2 T. N. Murakami and N. Koumura, *Adv. Energy Mater.*, 2019, **9**, 1802967.
3 B. O'Regan and M. Grätzel, *Nature*, 1991, **353**, 737–740.
4 A. Hagfeldt, G. Boschloo, L. Sun, L. Kloo and H. Pettersson, *Chem. Rev.*, 2010, **110**, 6595–6663.
5 A. Fakharuddin, R. Jose, T. M. Brown, F. Fabregat-Santiago and J. Bisquert, *Energy Environ. Sci.*, 2014, **7**, 3952–3981.
6 A. B. Muñoz-García, I. Benesperi, G. Boschloo, J. J. Concepcion, J. H. Delcamp, E. A. Gibson, G. J. Meyer, M. Pavone, H. Pettersson, A. Hagfeldt and M. Freitag, *Chem. Soc. Rev.*, 2021, **50**, 12450–12550.
7 H. Zhou, M. Aftabuzzaman, Masud, S. H. Kang and H. K. Kim, *ACS Energy Lett.*, 2025, **10**, 881–895.
8 Y. Ren, D. Zhang, J. Suo, Y. Cao, F. T. Eickemeyer, N. Vlachopoulos, S. M. Zakeeruddin, A. Hagfeldt and M. Grätzel, *Nature*, 2023, **613**, 60–65.
9 Y. Wu, W.-H. Zhu, S. M. Zakeeruddin and M. Grätzel, *ACS Appl. Mater. Interfaces*, 2015, **7**, 9307–9318.
10 P. Brogdon, H. Cheema and J. H. Delcamp, *ChemSusChem*, 2018, **11**, 86–103.
11 J.-M. Ji, H. Zhou and H. K. Kim, *J. Mater. Chem. A*, 2018, **6**, 14518–14545.
12 Y. Ren, D. Sun, Y. Cao, H. N. Tsao, Y. Yuan, S. M. Zakeeruddin, P. Wang and M. Grätzel, *J. Am. Chem. Soc.*, 2018, **140**, 2405–2408.
13 J.-M. Ji, H. J. Lee, H. Zhou, Y. K. Eom, C. H. Kim and H. K. Kim, *ACS Appl. Mater. Interfaces*, 2022, **14**, 52745–52757.
14 H. Imahori, T. Umeyama and S. Ito, *Acc. Chem. Res.*, 2009, **42**, 1809–1818.
15 T. Higashino and H. Imahori, *Dalton Trans.*, 2015, **44**, 448–463.
16 Y. Zhang, T. Higashino and H. Imahori, *J. Mater. Chem. A*, 2023, **11**, 12659–12680.
17 Y. Kurumisawa, T. Higashino, S. Nimura, Y. Tsuji, H. Iiyama and H. Imahori, *J. Am. Chem. Soc.*, 2019, **141**, 9910–9919.
18 Y. Zhang, T. Higashino, I. Nishimura and H. Imahori, *ACS Appl. Mater. Interfaces*, 2024, **16**, 67761–67770.
19 M. Urbani, M. Grätzel, M. K. Nazeeruddin and T. Torres, *Chem. Rev.*, 2014, **114**, 12330–12396.
20 A. Yella, H.-W. Lee, H. N. Tsao, C. Yi, A. K. Chandiran, M. K. Nazeeruddin, E. W.-G. Diau, C.-Y. Yeh, S. M. Zakeeruddin and M. Grätzel, *Science*, 2011, **334**, 629–634.
21 S. Mathew, A. Yella, P. Gao, R. Humphry-Baker, B. F. E. Curchod, N. Ashari-Astani, I. Tavernelli, U. Rothlisberger, M. K. Nazeeruddin and M. Grätzel, *Nat. Chem.*, 2014, **6**, 242–247.
22 A. Yella, C.-L. Mai, S. M. Zakeeruddin, S.-N. Chang, C.-H. Hsieh, C.-Y. Yeh and M. Grätzel, *Angew. Chem., Int. Ed.*, 2014, **53**, 2973–2977.
23 S. H. Kang, M. J. Jeong, Y. K. Eom, I. T. Choi, S. M. Kwon, Y. Yoo, J. Kim, J. Kwon, J. H. Park and H. K. Kim, *Adv. Energy Mater.*, 2017, **7**, 1602117.
24 J. Ji, H. Zhou, Y. K. Eom, C. H. Kim and H. K. Kim, *Adv. Energy Mater.*, 2020, **10**, 2000124.
25 H. Zhou, J.-M. Ji, H. S. Lee, Masud, M. Aftabuzzaman, D.-N. Lee, C. H. Kim and H. K. Kim, *ACS Appl. Mater. Interfaces*, 2023, **15**, 39426–39434.
26 H. Song, Q. Liu and Y. Xie, *Chem. Commun.*, 2018, **54**, 1811–1824.
27 S. Huang, Q. Li, S. Li, C. Li, H. Tan and Y. Xie, *Chem. Commun.*, 2024, **60**, 4521–4536.
28 K. Zeng, Y. Lu, W. Tang, S. Zhao, Q. Liu, W. Zhu, H. Tian and Y. Xie, *Chem. Sci.*, 2019, **10**, 2186–2192.
29 K. Zeng, Y. Chen, W.-H. Zhu, H. Tian and Y. Xie, *J. Am. Chem. Soc.*, 2020, **142**, 5154–5161.
30 Z. Li, Q. Lu, Y. Zhang, Q. Li, W. Wu, S. Li, H. Wang, J. Jiang, C. Li and Y. Xie, *J. Mater. Chem. A*, 2025, **13**, 4176–4185.
31 C.-C. Chen, J.-S. Chen, V. S. Nguyen, T.-C. Wei and C.-Y. Yeh, *Angew. Chem., Int. Ed.*, 2021, **60**, 4886–4893.
32 C.-C. Chen, Y.-H. Chen, V. S. Nguyen, S.-Y. Chen, M.-C. Tsai, J.-S. Chen, S.-Y. Lin, T.-C. Wei and C.-Y. Yeh, *Adv. Energy Mater.*, 2023, **13**, 2300353.
33 M. Wang, C. Grätzel, S. M. Zakeeruddin and M. Grätzel, *Energy Environ. Sci.*, 2012, **5**, 9394–9405.
34 J. Cong, X. Yang, L. Kloo and L. Sun, *Energy Environ. Sci.*, 2012, **5**, 9180–9194.

35 B. Pashaei, H. Shahroosvand and P. Abbasi, *RSC Adv.*, 2015, **5**, 94814–94848.
36 T. Higashino and H. Imahori, *ACS Energy Lett.*, 2022, **7**, 1926–1938.
37 C. E. Housecroft and E. C. Constable, *Chem. Sci.*, 2022, **13**, 1225–1262.
38 Masud and H. K. Kim, *ACS Omega*, 2023, **8**, 6139–6163.
39 Y. Saygili, M. Söderberg, N. Pellet, F. Giordano, Y. Cao, A. B. Muñoz-García, S. M. Zakeeruddin, N. Vlachopoulos, M. Pavone, G. Boschloo, L. Kavan, J.-E. Moser, M. Grätzel, A. Hagfeldt and M. Freitag, *J. Am. Chem. Soc.*, 2016, **138**, 15087–15096.
40 Y. Cao, Y. Liu, S. M. Zakeeruddin, A. Hagfeldt and M. Grätzel, *Joule*, 2018, **2**, 1108–1117.
41 Y. Ren, N. Flores-Díaz, D. Zhang, Y. Cao, J. Decoppet, G. C. Fish, J. Moser, S. M. Zakeeruddin, P. Wang, A. Hagfeldt and M. Grätzel, *Adv. Funct. Mater.*, 2020, **30**, 2004804.
42 D. Zhang, M. Stojanovic, Y. Ren, Y. Cao, F. T. Eickemeyer, E. Socie, N. Vlachopoulos, J.-E. Moser, S. M. Zakeeruddin, A. Hagfeldt and M. Grätzel, *Nat. Commun.*, 2021, **12**, 1777.
43 H. Rui, J. Shen, Z. Yu, L. Li, H. Han and L. Sun, *Angew. Chem., Int. Ed.*, 2021, **60**, 16156–16163.
44 S. M. Meethal, S. C. Pradhan, J. Velore, S. Varughese, R. S. Pillai, F. Sauvage, A. Hagfeldt and S. Soman, *J. Mater. Chem. A*, 2024, **12**, 1081–1093.
45 A. Colombo, G. Di Carlo, C. Dragonetti, M. Magni, A. Orbelli Biroli, M. Pizzotti, D. Roberto, F. Tessore, E. Benazzi, C. A. Bignozzi, L. Casarin and S. Caramori, *Inorg. Chem.*, 2017, **56**, 14189–14197.
46 T. Higashino, H. Iiyama, I. Nishimura and H. Imahori, *Chem. Lett.*, 2020, **49**, 936–939.
47 Y.-H. Chen, C.-C. Chen, V. S. Nguyen, X.-T. Jiang, Y.-D. Chen, M.-Y. Li, S.-Y. Chen, T.-C. Wei and C.-Y. Yeh, *Cell Rep. Phys. Sci.*, 2024, **5**, 102159.
48 T. Higashino, H. Iiyama, S. Nimura, Y. Kurumisawa and H. Imahori, *Inorg. Chem.*, 2020, **59**, 452–459.
49 G. C. Vougioukalakis, A. I. Philippopoulos, T. Stergiopoulos and P. Falaras, *Coord. Chem. Rev.*, 2011, **255**, 2602–2621.
50 L. Li, L. Zhao, X. Jiang, Z. Yu, J. liu, H. Rui, J. Shen, W. Sharmoukh, N. K. Allam and L. Sun, *J. Mater. Chem. A*, 2022, **10**, 4131–4136.
51 S. C. Pradhan, A. Hagfeldt and S. Soman, *J. Mater. Chem. A*, 2018, **6**, 22204–22214.
52 J. Ding, M. Day, G. Robertson and J. Roovers, *Macromolecules*, 2002, **35**, 3474–3483.
53 M. Karpacheva, F. J. Malzner, C. Wobill, A. Büttner, E. C. Constable and C. E. Housecroft, *Dye. Pigment.*, 2018, **156**, 410–416.
54 S. Kitagawa, M. Munakata and A. Higashie, *Inorg. Chim. Acta*, 1984, **84**, 79–84.
55 M. Giordano, G. Volpi, M. Bonomo, P. Mariani, C. Garino and G. Viscardi, *New J. Chem.*, 2021, **45**, 15303–15311.
56 P. Ferdowsi, Y. Saygili, S. M. Zakeeruddin, J. Mokhtari, M. Grätzel, A. Hagfeldt and L. Kavan, *Electrochim. Acta*, 2018, **265**, 194–201.
57 L. Kavan, Y. Saygili, M. Freitag, S. M. Zakeeruddin, A. Hagfeldt and M. Grätzel, *Electrochim. Acta*, 2017, **227**, 194–202.
58 G. Kalaignan and Y. Kang, *J. Photochem. Photobiol. C Photochem. Rev.*, 2006, **7**, 17–22.
59 N. V. Krishna, J. V. S. Krishna, M. Mrinalini, S. Prasanthkumar and L. Giribabu, *ChemSusChem*, 2017, **10**, 4668–4689.
60 J. M. Cole, G. Pepe, O. K. Al Bahri and C. B. Cooper, *Chem. Rev.*, 2019, **119**, 7279–7327.
61 Z. Li, Q. Li, C. Li and Y. Xie, *Mater. Chem. Front.*, 2024, **8**, 652–680.